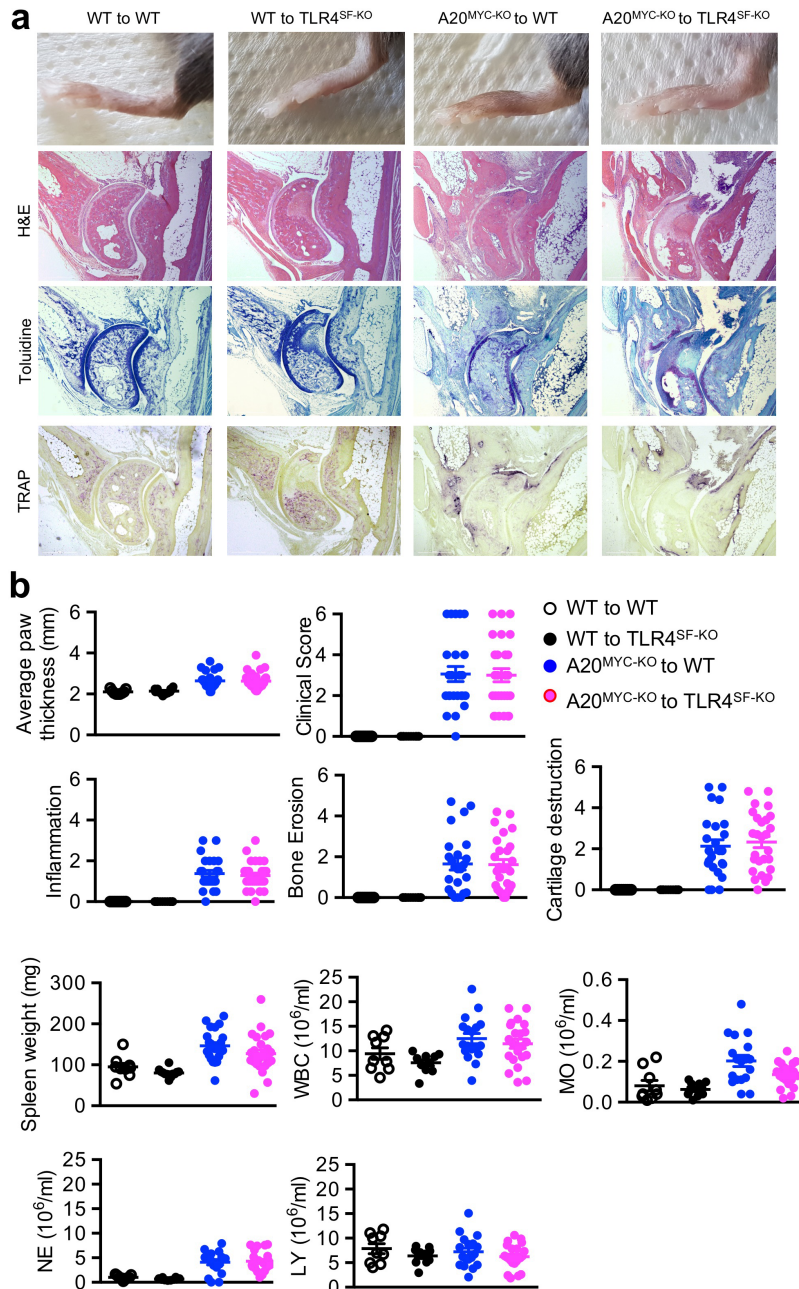**Supplementary Figure 1**

Leucocyte and cytokine analysis in the blood of wild type, A20^{MYC-KO}, A20^{MYC-KO} ASC^{MYC-KO}, A20^{MYC-KO} MyD88^{MYC-KO}, and A20^{MYC-KO} MyD88^{MYC} mice.

(a) Graphs indicating the number of white blood cells (WBC), lymphocytes (LY), monocytes (MO), and neutrophils (NE) in peripheral blood from mice with the indicated genotypes (wt, n=54; A20^{MYC-KO}, n=33; A20^{MYC-KO} Asc^{MYC-KO}, n=23 mice). (b) Levels of the indicated cytokines and chemokines in the serum of mice with the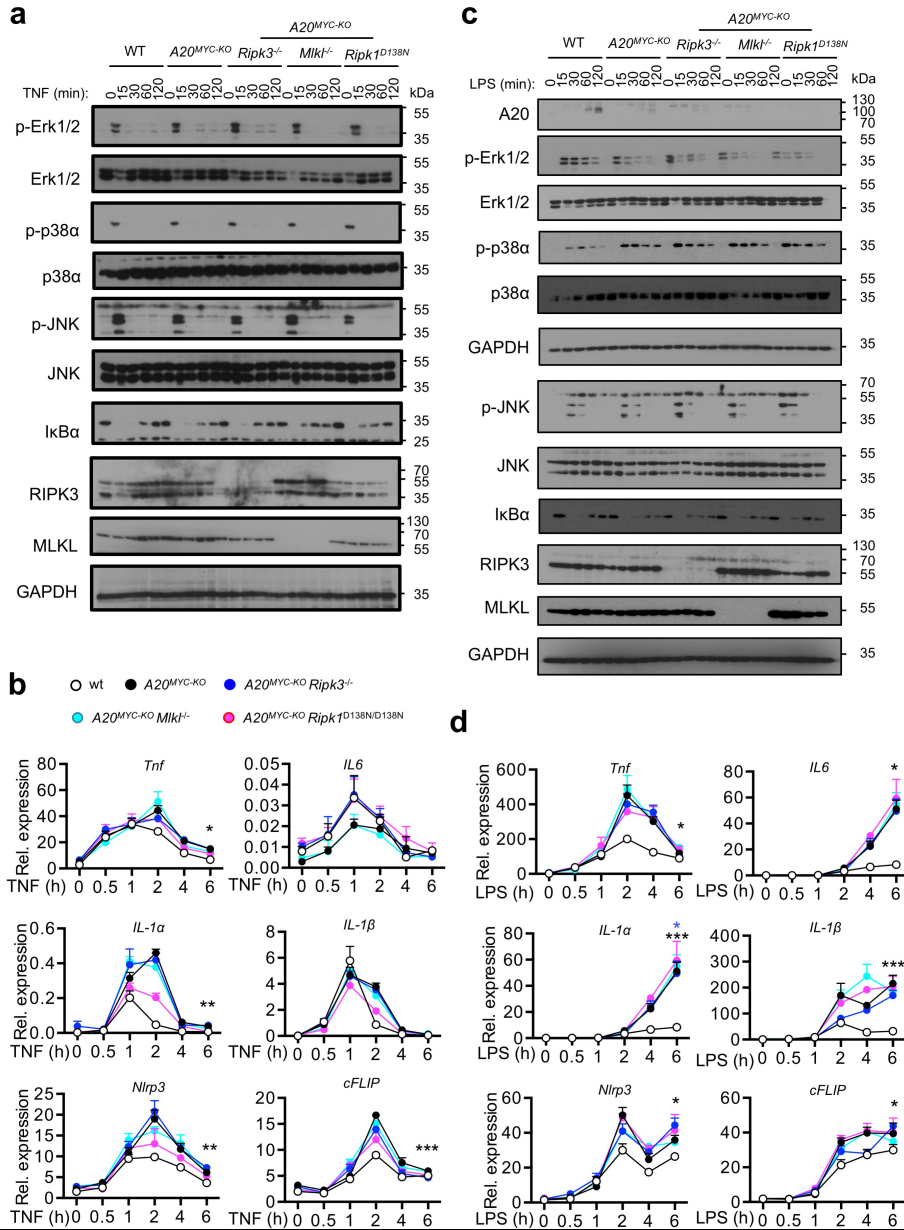 indicated genotypes (n=10 mice per genotype). (c) Graphs indicating the number of white blood cells (WBC), lymphocytes (LY), monocytes (MO), and neutrophils (NE) in peripheral blood from mice with the indicated genotypes. Wild type and A20^{MYC-KO} mice are the same shown in Supplementary Fig. 1 and are included for comparison (wt, n=54; A20^{MYC-KO}, n=33; A20^{MYC-KO} MyD88^{MYC-KO}, n=22; A20^{MYC-KO} MyD88^{MYC,} n=12 mice). (d) Levels of the indicated cytokines and chemokines in the serum of mice with the indicated genotypes (n=10 mice per genotype). Dots in the graphs indicate individual mice. In all graphs average ± SEM is also shown for each group of mice. *, ** and *** represent p<0.05, p<0.01 and p<0.001 respectively (one-way ANOVA with Bonferroni correction between indicated genotypes). All statistical tests are two-tailed. Raw data are provided in Supplementary Table 3.

Supplementary Figure 2

MyD88 regulates LPS- and IL-1β-induced inflammatory signalling in synovial fibroblasts.

a) Synovial fibroblasts with the indicated genotypes were stimulated with 1 µg/ml of LPS (left panel) or 10 ng/ml of IL-1β (right panel) and analysis of NF-κB and MAPK signalling was performed by immunoblotting with the indicated antibodies. Results of one representative out of two independent experiments are shown. (b-c) Synovial fibroblasts with the indicated genotypes were incubated with 1 µg/ml of LPS (b) or 10 ng/ml of IL-1β (c) and mRNA expression of the indicated genes was evaluated at the indicated time points after stimulation. Graphs depict pooled results from two independent experiments in which five independent isolations of synovial fibroblasts for each genotype (n=5 independent isolations of synovial fibroblasts) were used. (d) Graphs depicting spleen weight as well as the numbers of white blood cells (WBC), lymphocytes (LY), monocytes (MO), and neutrophils (NE) in peripheral blood from mice with the indicated genotypes. Dots indicate individual mice (wt to wt, n=7; wt to MyD88[SF-KO] n=8; A20[MYC-KO] to wt, n=11, A20[MYC-KO] to MyD88[SF-KO], n=10 mice). In all graphs average ± SEM is also shown for each group of mice. *, ** and *** represent p<0.05, p<0.01 and p<0.001 respectively (non-parametric Mann-Whitney test between indicated genotypes for d; two way ANOVA with Bonferroni correction for b, c). All statistical tests are two-tailed. Raw data are provided in Supplementary Table 3 and unprocessed immunoblots are provided in Supplementary Figure 9.

Supplementary Figure 3

Synovial fibroblast-specific TLR4 knockout does not inhibit arthritis caused by myeloid cell specific A20 deficiency
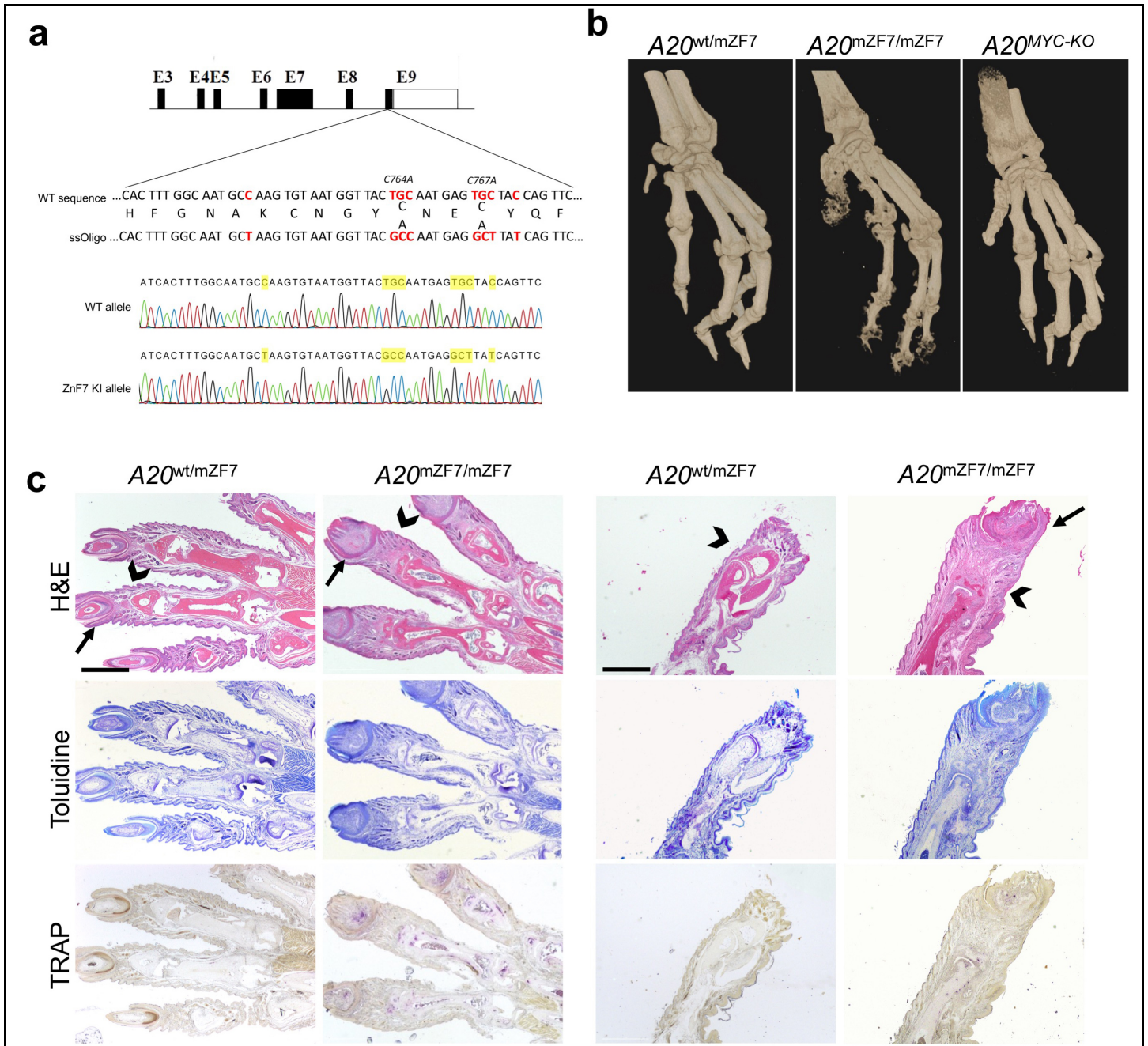
a) Representative macroscopic and histological images of the ankle joints of mice with the indicated genotypes analysed 32 weeks after adoptive transfer of bone marrow from wt or A20^{MYC-KO} animals (scale bar: 500μm). (b) Graphs depicting clinical scores, average thickness of rear paws at the ankle area, as well as histological scores for inflammation, bone erosion, and cartilage destruction in mice with the indicated genotypes transferred with bone marrow from wt or A20^{MYC-KO} animals. Dots in the graphs indicate individual mice (wt to wt, n=9; wt to TLR4^{SF-KO} n=12; A20^{MYC-KO} to wt, n=24, A20^{MYC-KO} to TLR4^{SF-KO}, n=27 mice for a-b). (c) Graphs depicting spleen weight, the number of white blood cells (WBC), lymphocytes (LY), monocytes (MO), and neutrophils (NE) in peripheral blood from mice with the indicated genotypes. (wt to wt, n=9; wt to TLR4^{SF-KO} n=10; A20^{MYC-KO} to wt, n=18, A20^{MYC-KO} to TLR4^{SF-KO}, n=22 mice). In all graphs average ± SEM is shown for each group of mice (non-parametric Mann-Whitney test between indicated genotypes). All statistical tests are two-tailed. Raw data are provided in Supplementary Table 3.

Supplementary Figure 4

RIPK3 or MLKL deficiency or lack of RIPK1 kinase activity, does not affect TNF- and LPS-induced NF-κB and MAPK activation as well as inflammatory gene expression in *A20*^{−/−} macrophages.

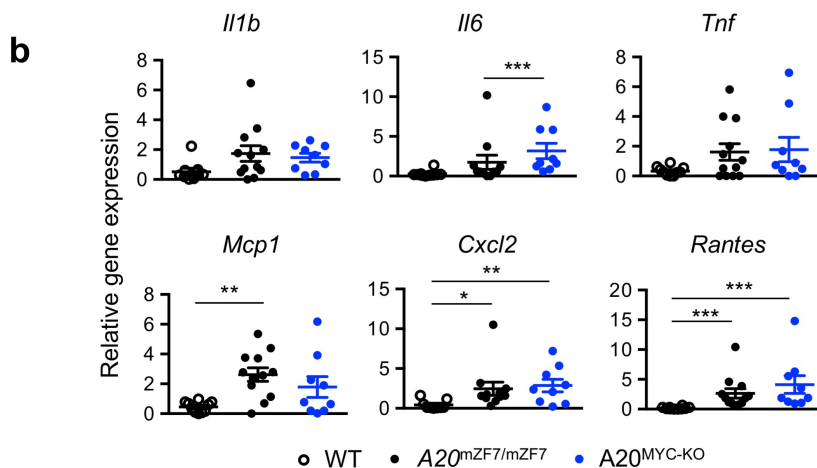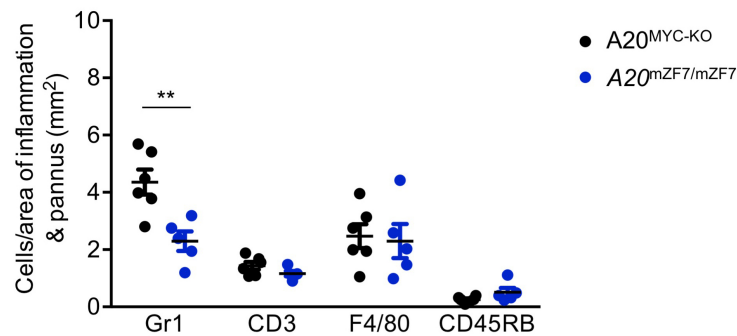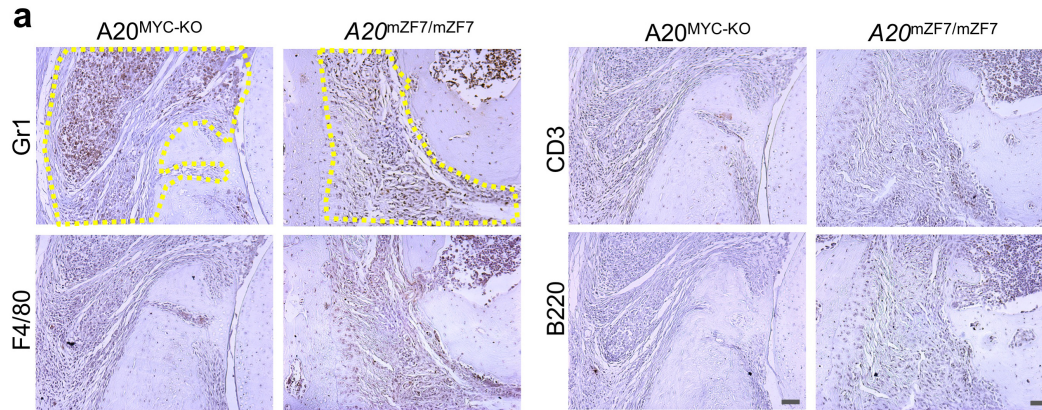(a-b) BMDMs with the indicated genotypes were stimulated with 20 ng/ml of TNF for the indicated time points. (a) Analysis of NF-κB and MAPK signalling was performed by immunoblotting with the indicated antibodies. Results of one representative out of two independent experiments are shown. (b) mRNA expression of the indicated genes was analysed by qRT-PCR Results shown were obtained from one experiment in which three independent isolations of BMDMs for each genotype (n=3 independent BMDM isolations) were included. (c-d) BMDMs with the indicated genotypes were stimulated with 20 ng/ml of LPS for the indicated time points. (c) Analysis of NF-κB and MAPK signalling was performed by immunoblotting with the indicated antibodies. Results of one representative out of two independent experiments are shown. (d) mRNA expression of the indicated genes was analysed by qRT-PCR. Results shown were obtained from one experiment in which three independent isolations of BMDMs for each genotype (n=3 independent BMDM isolations) were included. In all graphs average ± SEM is shown for each group of mice. *, ** and *** represent p<0.05, p<0.01 and p<0.001 respectively (two way ANOVA with Bonferroni correction). All statistical tests are two-tailed. Raw data are provided in Supplementary Table 3 and unprocessed immunoblots are provided in Supplementary Figure 9.

Supplementary Figure 5

$A20^{mZnF7/mZnF7}$ knock-in mice generated using CRISPR/Cas9-mediated gene targeting develop dactylitis.
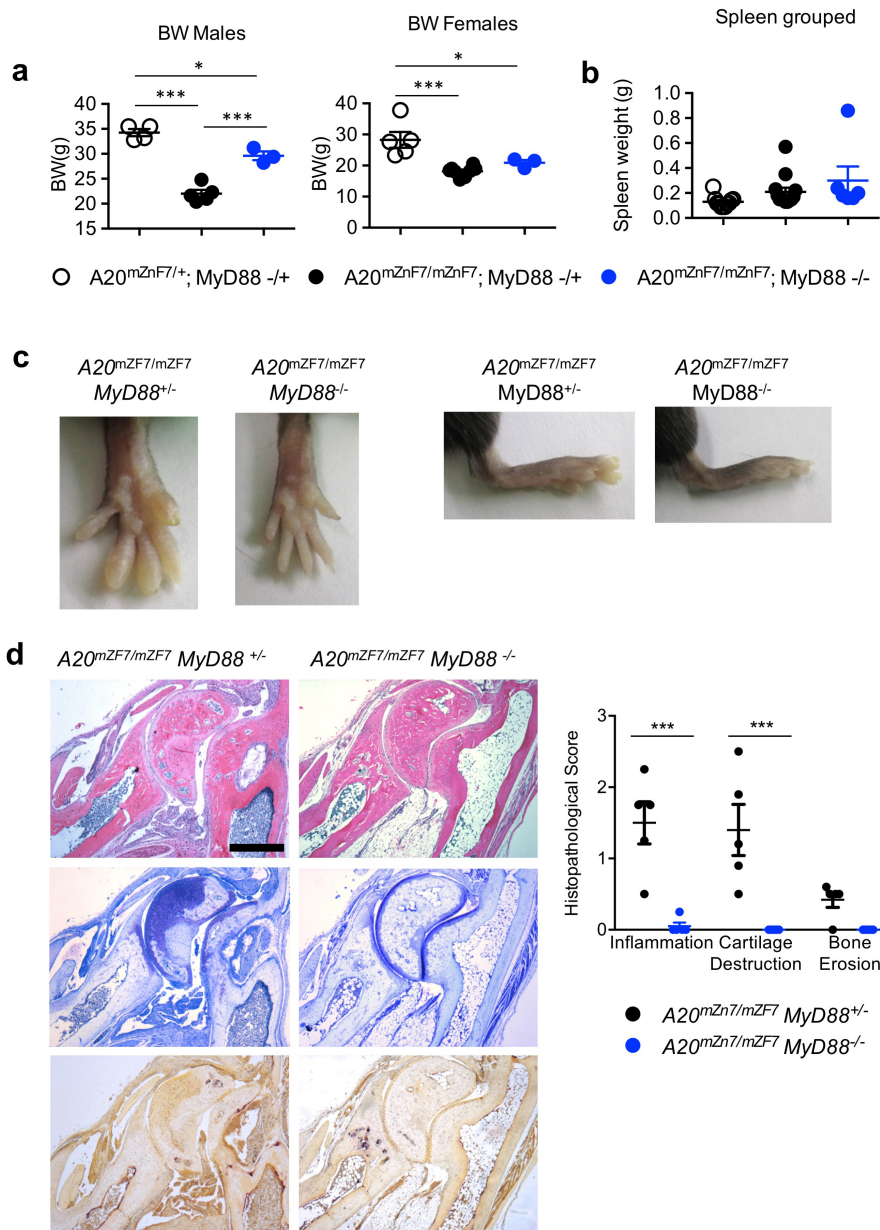
(a) Schematic representation of the A20 gene indicating the location of the point mutations introduced in exon 9 to change cysteine (C) residues at positions 764 and 767 to alanines (A). Two silent mutations were also introduced to avoid re-editing of the DNA by Cas9 after homology-directed repair. Sanger sequencing of wt and $A20^{mZnF7/mZnF7}$ mouse tail DNA to confirm correct introduction of the designed mutations into the genome. (b) mCT analysis of forepaws of mice with the indicated genotypes depicts the extensive bone erosions in the digits of $A20^{mZnF7/mZnF7}$ and the milder erosions in carpal bones compared to $A20^{MYC-KO}$ mice (c) Representative histological images from forepaws (right panel; transversal sections) and hindpaws (left panel; sagittal sections) of mice with the indicated genotypes. Note the development of dactylitis in $A20^{mZnF7/mZnF7}$ mice with a characteristic severe tenosynovitis leading to disruption of muscle/tendon fibres and the pannus orchestrating destruction of bones (arrow), all being more evident in the distal and intermediate (arrowhead) than in proximal phalanxes (scale bar: 1mm) ($A20^{wt/mZnF7}$, n=8 and $A20^{mZnF7/mZnF7}$, n=10 mice).

a

A20^MYC-KO   *A20*^mZF7/mZF7   A20^MYC-KO   *A20*^mZF7/mZF7

Gr1

F4/80

CD3

B220

- A20^MYC-KO
- *A20*^mZF7/mZF7

Cells/area of inflammation & pannus (mm^2)

Gr1   CD3   F4/80   CD45RB

b

Il1b   *Il6*   *Tnf*

Relative gene expression

Mcp1   *Cxcl2*   *Rantes*

○ WT   ● *A20*^mZF7/mZF7   ● A20^MYC-KO

Supplementary Figure 6

Comparison of immune cell infiltration and inflammatory cytokine and chemokine expression in joints from A20^MYC-KO and *A20*^mZnF7/mZnF7 mice.
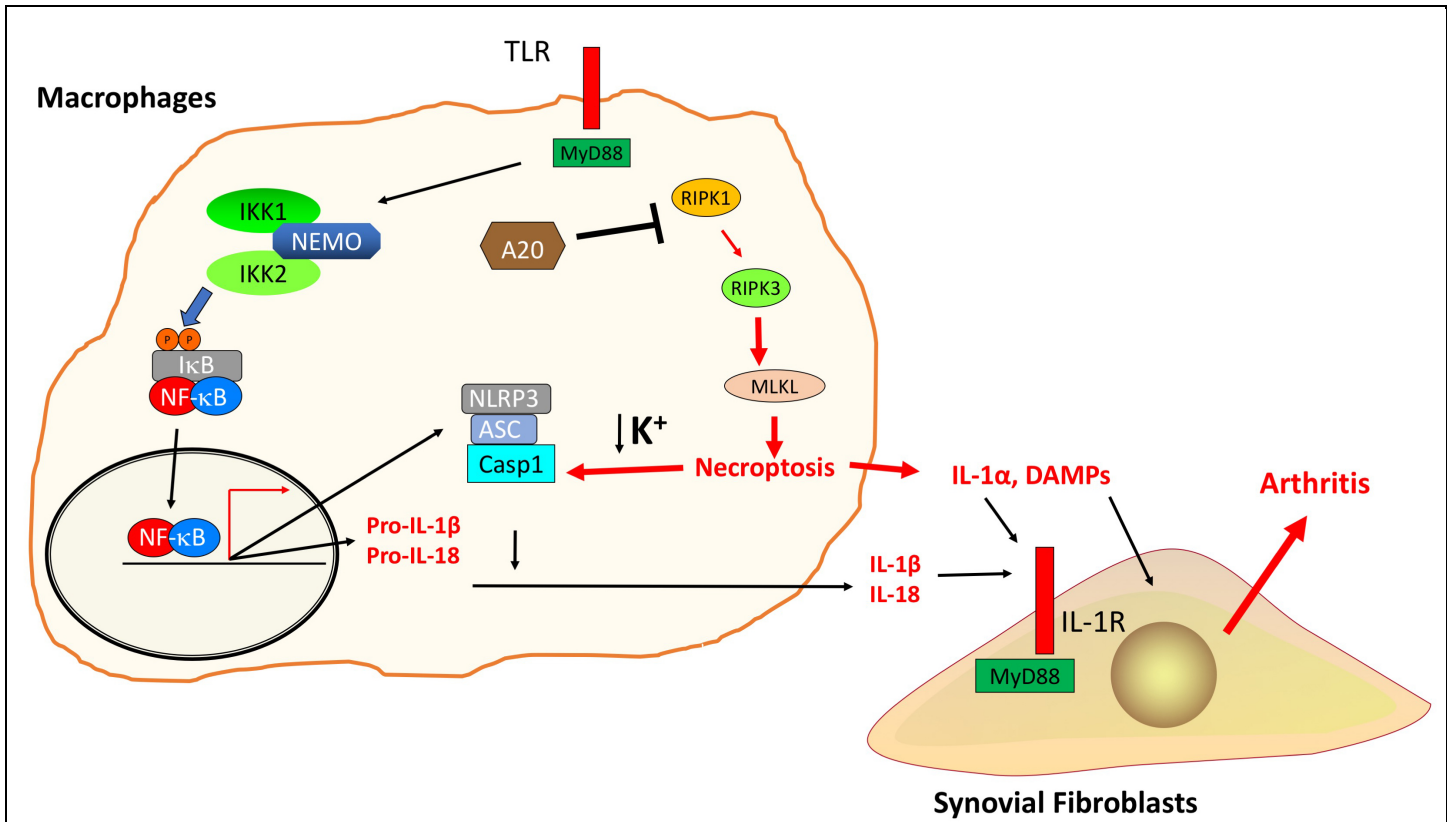
(a) Representative images of histological serial sections from the ankle joints of mice with the indicated genotypes, which were immunostained with the indicated antibodies (*A20*^MYC-KO ,n=6 and *A20*^ZnF7 n=5 mice). Immune cell numbers were evaluated within the affected areas (dotted line). Data represents mean ± SEM (non-parametric Mann-Whitney test between indicated genotypes).   (b) The mRNA expression of the indicated cytokines and chemokines was analyzed by qRT-PCR in RNA from hind paws of mice with the indicated genotypes. Each dot represents an individual mouse (*A20*^wt/wt, n=9-10*; A20*wt/mZnF7, n=11-12 and *A20*^MYC-KO, n=9 mice). Average ± SEM is also shown for each group of mice. *, ** and *** represent p<0.05, p<0.01 and p<0.001 respectively (Kruskal-Wallis one-way ANOVA test between indicated genotypes). All statistical tests are two-tailed. Raw data are provided in Supplementary Table 3.

Supplementary Figure 7

MyD88 deficiency prevents the development of arthritis and dactylitis in $A20^{mZnF7/mZnF7}$ mice.

a) Graphs depicting the body weight (BW) of mice with the indicated genotypes at the age of 20-30 weeks. (b) Graph depicting spleen weight of mice with the indicated genotypes. (c) Representative pictures of forepaws and hindpaws of mice with the indicated genotypes at the age of 20 weeks. (d) Representative histological images of ankle joints from 20-30-week-old littermate mice with the indicated genotypes. Scale bar: 500 μm. Graph depicts histological scores for inflammation, bone erosion, and cartilage destruction in mice with the indicated genotypes. Dots in the graphs indicate individual mice ($A20^{mZnF7/+}$ $MyD88^{-/+}$ n=4; $A20^{mZnF7/mZnF7}$ $MyD88^{-/+}$ n=5; $A20^{mZnF7/mZnF7}$ $MyD88^{-/-}$ n=3 mice for a,b; $A20^{mZnF7/mZnF7}$ $MyD88^{-/+}$ n=5; $A20^{mZnF7/mZnF7}$ $MyD88^{-/-}$ n=5 mice for d). In all graphs average ± SEM is also shown for each group of mice. *, **, and *** represent p<0.05, p<0.01, and p<0.001 respectively (One-way ANOVA with Bonferroni correction for a; two-way ANOVA with Bonferroni correction for b). All statistical tests are two-tailed. Raw data are provided in Supplementary Table 3.

Supplementary Figure 8

Schematic model depicting the mechanisms regulating the pathogenesis of inflammatory arthritis in A20^{MYC-KO} mice.

A20 prevents inflammasome activation and the release of mature IL-1β and IL-18 but also IL-1α in macrophages by inhibiting RIPK1-RIPK3-MLKL-dependent necroptosis. In A20-deficient macrophages, RIPK1-RIPK3-MLKL-dependent signalling causes necroptosis that results in the release of IL-1α and other DAMPs. In addition, MLKL-dependent plasma membrane permeabilization triggers K+ efflux, which activates the NLRP3 inflammasome and the caspase-1-dependent processing and subsequent release of IL-1β and IL-18. IL-1α and IL-1β, likely together with IL-18 and other DAMPs released by necroptotic A20-deficient macrophages activate MyD88-dependent proinflammatory signalling in synovial fibroblasts causing joint tissue inflammation, as well as cartilage and bone destruction resulting in the development of arthritis.